Anchoring ultrafine Pt electrocatalysts on TiO$_2$-C via photochemical strategy to enhance the stability and efficiency for oxygen reduction reaction

Jingyu Wang[a,*], Min Xu[a], Jianquan Zhao[b], Huaifang Fang[c], Qingzhu Huang[c], Weiping Xiao[a], Tao Li[a,*], Deli Wang[a,*]

[a] Key Laboratory of Material Chemistry for Energy Conversion and Storage (Ministry of Education), School of Chemistry and Chemical Engineering, Huazhong University of Science and Technology, Wuhan, 430074, Hubei, China
[b] Analysis and Testing Center, Huazhong University of Science and Technology, Wuhan, 430074, Hubei, China
[c] College of Chemistry and Materials Science, South-Central University for Nationalities, Wuhan, 430074, Hubei, China

A R T I C L E   I N F O

A B S T R A C T

The activity and stability of Pt electrocatalysts are crucial issues for energy conversion systems involving oxygen reduction reaction (ORR). In this work, the ultrafine Pt nanoparticles were in situ reduced by the photogenerated electrons on TiO$_2$ surface so that most of them selectively anchored around the TiO$_2$ nanocrystals. The presence of well-dispersed TiO$_2$ on carbon surface strengthened the metal-support interaction, giving rise to the improved ORR catalytic activity with ∼ 49 mV positive shift of half-wave potential as compared to commercial 20 wt% Pt/C. More importantly, the Pt/TiO$_2$-C catalysts exhibited a more durable performance after 10,000 cycles in terms of the decrease in electrochemical surface area (0.8%) and mass activity (0.9%), much lower than those of Pt/C (10.2% and 33.3%). The high-temperature durability test also revealed a much higher retention of ORR activity. The results demonstrated that anchoring Pt on well-dispersed TiO$_2$-decorated carbon would be an effective strategy to enhance the ORR performance by strong metal-support interaction, which facilitated the electron transfer during catalytic reactions as well as prevented Pt aggregation during durability test.

1. Introduction

Polymer electrolyte membrane fuel cells (PEMFCs) have been widely investigated as promising energy conversion systems to produce electricity due to their pollution-free process and high efficiency (∼80%). It is well-known that the activity and durability of the electrode materials for oxygen reduction reaction (ORR) are crucial to the large-scale commercialization of PEMFCs technology [1]. Currently, the most widely used catalysts are depositing Pt-based materials on carbon support to reduce the consumption of such precious metal [2–5]. Although the carbon material possesses the merits of low cost and high electrical conductivity, it usually suffers from low durability because of the severe corrosion under harsh operation conditions of fuel cells and weak metal-support interactions. These drawbacks bring about the agglomeration of Pt catalysts and the resulting decrease of electrocatalytic activity [6–8].

In general, the requirements for an ideal ORR catalyst include high stable support with tolerance to strong oxidative and acidic/alkaline conditions, strong interactions between catalyst and support, and uniform dispersion of ultrafine Pt crystals [6,9,10]. Titanium oxide has

been extensively studied in various catalytic systems owing to its low cost, high chemical/thermal/photo- stability, environmental friendliness, etc [11–14]. The strong corrosion resistance ensures TiO$_2$ to be an intrinsically stable electrode material under harsh operation conditions, especially in acidic medium and high-temperature environment [15–17]. Its another attractive property is known as strong metal-support interaction (SMSI), which has been discovered in many metal-semiconductor hybrid structures [18–20]. The SMSI effect comes from the electronic interactions, hence it not only improves the durability of Pt catalysts but also favors the electrons transferring from the support to the catalyst [15,21,22]. Most importantly, as a typical semiconductor photocatalyst, TiO$_2$ nanocrystals (NCs) can be excited by light irradiation to generate electrons, which will directly reduce the Pt(IV) to metallic Pt nanoparticles (NPs) without the use of any reducing reagents.

It is noted that the typical synthetic procedures of nano-sized Pt catalysts usually employ reducing agents such as polyols or reducing gas such as H$_2$ at elevated temperature [23–28]. In some cases, the surfactants are also introduced to restrain the aggregation of Pt crystals [29,30]. Most recently, very few literatures reported the photochemical

synthesis of Pt electrocatalyst on the support containing semiconductor photocatalyst. Under light irradiation, the ultrafine Pt NPs are in situ reduced and highly dispersed on the surface of semiconductor NCs owing to the uniformly generated electrons and moderate reduction process [31–33]. In comparison to typical reduction methods, the photochemical strategy yields Pt NPs using the photogenerated electrons of the support instead of additional reducing agents such as polyols or H_2. Moreover, the direct electronic interaction with the semiconductor will strengthen the SMSI effect, which gives rise to the improvement of catalytic activity and durability of Pt electrocatalyst. Hence the development of such a green and energy-saving strategy is expected to facilitate the utilization of the resourceful solar energy for electrocatalytic applications.

As for the photocatalyst-containing support, the main obstacle is the low electrical conductivity and poor reactivity of the semiconductors like TiO_2 [34]. Several groups increased the electrical conductivity of TiO_2 by doping with transition metal (Mo, Nb, V, etc.), surface hydrogenation, coupling with heteroatoms-doped carbon or carbon nanotubes (CNT) [6,15,35–39]. These attempts indeed improved the long-term durability of Pt catalysts; some of which also achieved more efficient ORR catalytic activity than commercial Pt/C (Com. Pt/C) from one of aspects such as onset potential (E_O), half-wave potential ($E_{1/2}$) or electrochemical surface area (ECSA). The incorporation of TiO_2 semiconductor with carbon materials is reported to be one of the most effective solutions to improving its low electrical conductivity [38–40]. Badam et al employed the photochemical route to prepare Pt NPs on CNT-TiO_2 supports, however, the catalysts displayed lower values of $E_{1/2}$ and ECSA than Com. Pt/C. The durability test is absent in their work [40].

Based on the above mentioned critical factors on the catalysts' performance, we designed a TiO_2-C composite support with well-dispersed TiO_2 NCs on carbon surface. Benefiting from the function of TiO_2 as photocatalysts, the ultrafine Pt NPs were in situ reduced and mostly surrounded the TiO_2 NCs with well-dispersion during the photochemical reduction process. In this case, the direct electronic interactions between Pt and TiO_2, favourable to the SMSI effect, are naturally formed and thus result in the enhanced catalytic activity and durability through the comprehensive comparisons in E_O, $E_{1/2}$, ECSA, and durability at both room and high temperature.

2. Experimental

2.1. Materials

Nitric acid (65.0%–68.0%), hydrochloric acid (36.0%–38.0%), methanol, ethanol, isopropanol and tetrabutyl titanate (TBT), are obtained from National Medicines Corporation Ltd. of China. Nafion solution (DuPont, 5 wt%). Vulcan carbon black (XC-72), commercial 20 wt% Pt/C, and chloroplatinic acid hexahydrate are obtained from Aladdin. All of reagents are of analytical grade.

2.2. Synthesis of TiO₂-C composite support

The Vulcan XC-72 was pretreated by refluxing in hydrochloric acid [HCl:water = 1:5 (volume ratio)] and then in 5 M nitric acid. After acidization, the precipitation were collected by centrifugation, washing, drying at 150 °C for 8 h. 500 mg of acidized carbon powders were dispersed in 30 ml of water and ultrasonicated for 30 min. Then the TiO_2-C composite was synthesized using a liquid-phase assembly process. 3 ml of TBT was dissolved in 22 ml of absolute ethanol, and then was added dropwise into the above suspensions of carbon and water under magnetic stirring at room temperature. After complete addition, the suspension was mechanically agitated at 70 °C for about 1.5 h to obtain a condensed suspension. 70 ml of 0.055 M HNO_3 was then added into the suspension, and the mixture was refluxing at 70 °C under stirring for 4 h. The precipitation was collected by centrifugation,

washing with ethanol and deionized water, and finally vacuum drying at 60 °C for 12 h. The final product was obtained by heating in a tube furnace at 400 °C with a heating rate of 2 °C min^{-1} under flowing N_2 for 2 h.

2.3. Synthesis of Pt/TiO₂-C electrocatalysts

Pt NPs were loaded on TiO_2-C support by photochemical deposition process. 20 mg of TiO_2-C was added into the mixture of 40 ml of H_2O and 10 ml of methanol. After ultrasonication for 15 min, 210 μL of 0.0193 M H_2PtCl_4·$6H_2O$ were added and the suspensions were stirring at 30 °C under flowing N_2. The A 250 W high pressure mercury lamp was used as the light source to initiated the photoreduction process during 5 h irradiation. 210 μL of H_2PtCl_4·$6H_2O$ and 5 ml of methanol were supplemented in the reaction system after every hour.

For comparison, the Pt/TiO_2-C (polyol) and Pt/TiO_2-C (H_2) catalysts were prepared by typical reduction methods using polyol and H_2 as reduction reagents. (1) Pt/TiO_2-C (polyol): 20 mg of TiO_2-C was suspended in 40 mL of ethylene glycol solution by ultrasonic treatment for 30 min. 533 μL of 0.0193 M H_2PtCl_4·$6H_2O$ were added dropwise and then the solution was refluxing at 140 °C for 4 h under mechanical stirring. (2) Pt/TiO_2-C (H_2): 20 mg of TiO_2-C was suspended in 10 mL of H_2O containing 533 μL of 0.0193 M H_2PtCl_4·$6H_2O$. After ultrasonic treatment for 15 min, the suspension was stirring at 60 °C for 2 h. Then solid product was collected, washed, and heated in a tube furnace at 300 °C under flowing H_2/N_2 for 2 h.

2.4. Characterization

XRD patterns were recorded by X-ray powder diffraction (XRD) (PANalytical B.V.) equipped with Cu Kα irradiation at 40 kV and a diffracted beam monochromator at 40 mA. Transmission electron microscopy (TEM) and high-resolution transmission electron microscopy (HRTEM) images were obtained by a Tecnai G^2 F30 transmission electron microscope (FEI, Netherlands). The nitrogen adsorption and desorption isotherms were obtained using an ASAP 2020 (Micromeritics Instruments, USA) nitrogen adsorption apparatus. The X-ray photoelectron spectroscopy (XPS) measurements were performed on AXIS-ULTRA DLD-600 W. The Fourier transform infrared (FT-IR) spectra were acquired on a VERTEX 70 in a KBr tablets, scanning from 4000 to 400 cm^{-1} at room temperature. Raman spectra were collected on a labRAM HR800 (France, Jobin Yvon) Raman spectrometer over a range from 100 cm^{-1} to 2000 cm^{-1}. The actual loading amount of Ti and Pt was measured by inductively coupled plasma-mass spectrometry (ICP-MS). The thermogravimetric analyses (TGA) were performed on a Pyris1 TGA (PerkinElmer Instruments) in air, with the temperature ranging from 25 to 800 °C, at a heating rate of 10 °C min^{-1}.

2.5. Electrochemical measurements

4 mg of electrocatalysts were dispersed in 16 μL of Nafion solution (5 wt%) and 0.8 mL of isopropanol, which was followed by ultrasonication for 30 min to form a homogeneous ink. Then, a certain amount of ink was loaded on a glassy carbon rotating disk electrode (RDE, 5 mm in diameter, Pine Instruments). The Pt loading mass on RDE was normalized as 20.4 μg cm^{-2}. A Pt wire was used as the counter electrode and a reversible hydrogen electrode (RHE) was used as the reference electrode. The CV curve was recorded at room temperature in a N_2-saturated 0.1 M $HClO_4$ solution in the potential range of 0.05–1.2 V (versus RHE) at a scanning rate of 50 mV s^{-1}. The ORR catalytic activities were measured at room temperature in an O_2-saturated 0.1 M $HClO_4$ and 0.1 M KOH solution through the RDE method at a scanning rate of 5 mV s^{-1} and a rotating rate of 1600 rpm. The accelerated durability test was performed by cycling the catalyst in the potential range of 0.6–1.0 V (versus RHE) at a rate of 100 mV s^{-1} for 10,000 scans in O_2-saturated 0.1 M $HClO_4$ solution. The stability of

catalysts is evaluated at both room-temperature and high-temperature (60 °C). The slopes of the linear lines were used to calculate the number of electrons transferred (*n*) according to the following Koutecky–Levich equation [41,42].

$$1/J = 1/J_k + 1/J_d = 1/J_k + 1/(B\omega^{1/2})$$

$$B = 0.62 \; nFC_O D_O^{2/3} \nu^{-1/6}$$

Where *J* is the measured current density, J_k and J_d are the kinetic- and diffusion-limiting current densities, ω is the angular velocity, *n* is transferred electron number, *F* is the Faraday constant (F = 96,485 C mol^{-1}), C_O is the concentration of O_2 in electrolyte, D_O is the O_2 diffusion coefficient, ν is the kinematic viscosity of the electrolyte.

CO-stripping tests were conducted in 0.1 M $HClO_4$ electrolyte. Before recording, two CVs cycles from 0.05 to 1.2 V (versus RHE) was performed at 5 mV s^{-1} to ensure the steady-state condition. CO was adsorbed at 0.1 V in CO-saturated electrolyte for 10 min, and further purged for 30 min with N_2. Two potential cycles from 0.05 to 1.2 V were recorded at a scan rate of 50 mV s^{-1}. Electrochemical impedance spectroscopy (EIS) was measured as follows. 2 mg of catalyst was dispersed in 1 mL of water and then 75 μL of the suspension was dip-coated on the ITO glass electrode. After drying the electrode, EIS was measured in 0.1 M KCl solution containing 5 mM $Fe(CN)_6^{3-}$/$Fe(CN)_6^{4-}$ at the open circuit potential.

3. Results and discussion

The fabrication process of Pt/TiO_2-C catalysts is illustrated in Fig. 1. The carbon black was pre-treated by acid to generate more oxygen-containing functional groups on the surface. As reported by literatures, the HCl and HNO_3 pre-treatment will increase the concentration of hydroxyl and carboxyl groups on the carbon surface, respectively [43]. The activation of the carbon surface promote the uniform decoration of metal or metal oxide NPs on the surface [38,44]. In this way, the TiO_2 nanocrystals were uniformly dispersed on the carbon surface to form the TiO_2-C composite during the liquid-phase assembly process. Finally, the $PtCl_6^{2-}$ ions were reduced to ultrafine Pt NPs by the photo-generated electrons on the TiO_2 surface under light irradiation.

The XRD patterns in Fig. 2a show the characteristic diffraction peaks of anatase TiO_2 according to the standard JCPDS card No. 21-1272. The incorporation with carbon black has negligible influence on the crystal phase or size of TiO_2 NCs. Four additional peaks at 39.6°, 46.1°, 67.2° and 80.9° are assigned to face-centred cubic (fcc) Pt (JCPDS card No. 87-0642). Using Scherrer's formula, the average crystal sizes of TiO_2 and Pt NPs are estimated to be ~9.5 and ~3.5 nm, respectively. From TEM observation in Fig. 2b-e, the smooth surface of carbon materials was uniformly decorated by well-dispersed TiO_2 and Pt NPs. According to analysis of nitrogen adsorption – desorption isotherms, the decoration of TiO_2 caused the specific surface area of carbon black to increase from 125.6 to 190.0 m^2 g^{-1} (Fig. S1 and Table S1), implying the well-dispersed TiO_2 NCs on carbon surface. The surface elemental

distribution of Pt/TiO_2-C was determined by EDX measurement (Fig. 2d), confirming the coexistence of Pt and Ti on the carbon surface with a Pt:Ti atomic ratio of 1:1.6. The obtained Pt NPs display a narrow size distribution of approximate 3.2 ± 0.5 nm (Fig. 2f). The particle size of 3–4 nm is generally known to be superior for the catalytic efficiency of Pt electrocatalysts [45–47]. Fig. 2g shows the HRTEM image of Pt/TiO_2-C, which is magnified in Fig. 2h. The distinct lattice fringe with an interplanar spacing of 0.352 nm corresponds to the TiO_2(101) plane, whereas the lattice spacing of 0.226 nm is assigned to the Pt(111) plane. It is very clear that most of the ultrafine Pt NPs are grown around the TiO_2 surface by photochemical reduction. Therefore, the obtained Pt NPs, with appropriate size distribution and the location on TiO_2 surface, are expected to benefit the ORR catalytic activity and stability.

XPS technique was adopted to study the chemical states of the elements in the TiO_2, TiO_2-C, and Pt/TiO_2-C. The survey spectra demonstrate the present of each element in the composite (Fig. S2). The high-resolution XPS spectrum of C 1s can be deconvoluted to three peaks at 290.0, 286.1, and 285.0 eV (Fig. 3a), corresponding to the C= O, C−O, and C−C, respectively [48]. The high-resolution O 1s spectrum in Fig. 3b displays a predominant peak at 530.7 eV (Ti−O) with a shoulder peak at 532.4 eV (−OH). The Ti 2p spectrum of pure TiO_2 shows doublet peaks at 464.3 and 458.6 eV with a spin-orbital doublet splitting of 5.7 eV, indicating the chemical state of Ti^{4+} in TiO_2 (Fig. 3c). The binding energy locations are consistent with the anatase TiO_2 in our previous studies [49]. In contrast, the binding energy of Ti 2p in TiO_2-C is 0.8 eV higher than that of pure TiO_2. After the deposition of Pt NPs, the locations further shifted to 0.2 eV higher energy value. Such higher shift is induced by the electronic interaction decreasing the electron intensity on the Ti atom [49,50]. That is, there are strong interactions of TiO_2 with both carbon and Pt NPs in the Pt/TiO_2−C composite. As further evidence, the presence of carbon also caused the absorption band of Ti−O−Ti stretching vibrations in the FTIR spectrum to shift to lower wavenumber (Fig. S3). The effect of deposited Pt NPs on the electronic properties of TiO_2 can be revealed by Raman spectroscopy (Fig. 4a). The obvious red shift of the characteristic scatterings of anatase TiO_2 verifies the interaction between Pt and TiO_2. According to CO stripping voltammograms, the CO oxidation peak of Pt/TiO_2-C displays the negative shift of 130 mV by reference to Com. Pt/C (Fig. 4b), also suggesting the altered electronic property of Pt electrocatalyst by TiO_2 [51]. Hence the introduction of TiO_2 NCs strengthened the SMSI effect, which was favorable for the electrons transferring from the support to the catalyst and stabilization of the Pt catalysts [15,21,22]. The Pt 4f spectrum shows two distinct doublet peaks of Pt $4f_{5/2}$ and $4f_{7/2}$, each of which can be resolved into three peaks (Fig. 3d). The locations at 73.4, 72.3, and 71.4 eV are assigned to Pt^{IV}, Pt^{II}, and Pt$^{\circ}$, respectively [39]. The Pt$^{\circ}$ is the predominant state with the proportion of 52.4%, suggesting that most of Pt^{IV} ions were reduced to metallic Pt$^{\circ}$ NPs by the photogenerated electrons on the TiO_2 surface. The Pt 4f spectrum of commercial Pt/C was also measured for comparison. As shown in Fig. 3d, the binding energy of Pt 4f in Pt/TiO_2-C is 0.4 eV lower than that of Com. Pt/C. The lowered binding energy
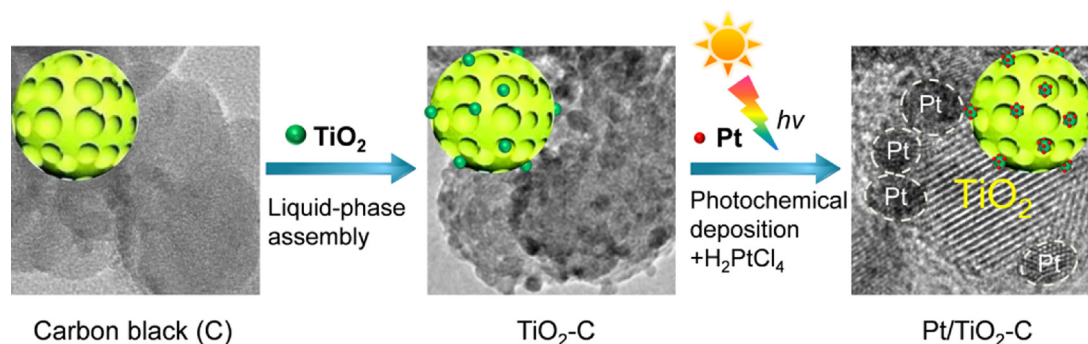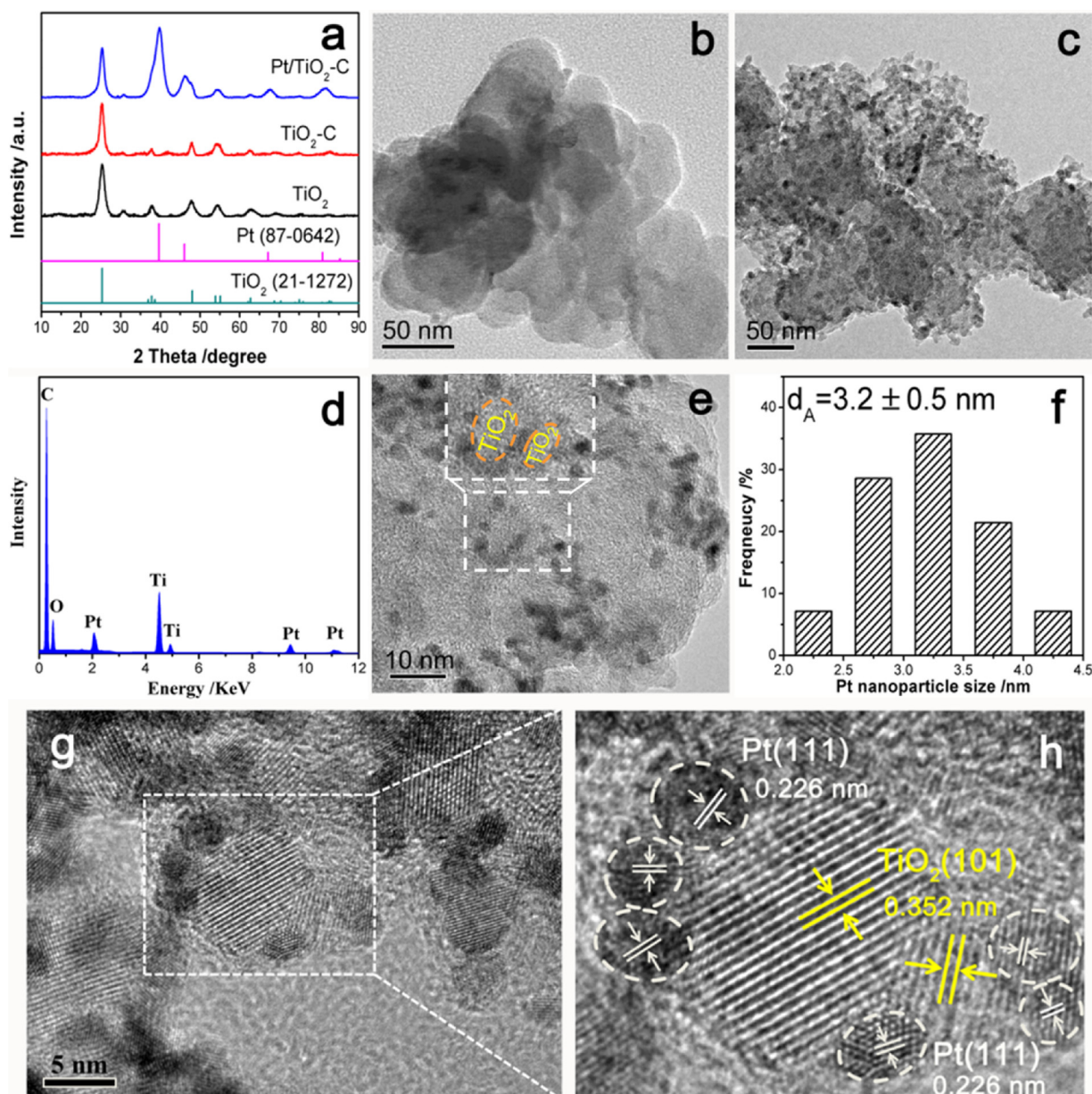

Fig. 1. The fabrication process of Pt/TiO_2-C catalysts.

Fig. 2. (a) XRD patterns of as-prepared TiO$_2$, TiO$_2$-C, and Pt/TiO$_2$-C. TEM images of (b) carbon black (Vulcan XC-72) and (c) Pt/TiO$_2$-C. (d) EDX spectrum of Pt/TiO$_2$-C. (e) Magnified TEM image of Pt/TiO$_2$-C. (f) The Pt particle size distribution of Pt/TiO$_2$-C. (g) HRTEM image of Pt/TiO$_2$-C. (h) The magnification of the selected area in (g).

value of Pt 4f is also the result of SMSI effect by accepting the electrons from TiO$_2$.

The influence of TiO$_2$ on the electrocatalytic performance of Pt NPs was studied by electrochemical measurements. To normalize the Pt loading, the compositions of the catalysts were measured by ICP-MS. The obtained Pt/TiO$_2$-C composite consists of 26.4 wt% TiO$_2$ and 6.9 wt % Pt. According to the theoretical amount of Pt, the yield of Pt electrocatalyst in the composite is calculated to be 34.5%. As further evidence, the TG curves of TiO$_2$-C and Pt/TiO$_2$-C are plotted in Fig. S4, which is in good agreement with ICP-MS analysis. Fig. 5a shows CV curves of samples in N$_2$-saturated 0.1 M HClO$_4$ at a scan rate of 50 mV s^{-1}. The onset and peak potentials of surface oxide reduction on Pt/ TiO$_2$-C electrode are both positive than those of commercial (Com.) Pt/ C. The shifts further confirm that the Pt NPs have been successfully deposited on the surface of TiO$_2$ and thus the strong interaction with TiO$_2$ modified the electronic structure of Pt, causing a weak oxygen affinity of Pt catalysts [52,53]. At the same mass loading of Pt catalyst,

the electrochemical surface area (ECSA) values are calculated by integrating the charges in the hydrogen desorption region, corresponding to desorption of a monolayer of hydrogen from Pt surfaces (Fig. 5b). The Com. Pt/C, i.e., 20 wt% Pt loading on Vulcan XC72 carbon black, possesses an ECSA value as 77.14 m^2 g$_{Pt}^{-1}$, which agrees with the recent reports [54–56]. When loading Pt NPs on TiO$_2$-C, the CV curve displays no additional current peaks but the wider H$_2$ adsorption/desorption area. This means that TiO$_2$ is electrochemically inert to be a good support under the operation conditions of fuel cells. The ECSA slightly increased to 81.67 m^2 g$_{Pt}^{-1}$, suggesting the better electrochemical activity than Com. Pt/C.

To evaluate the catalytic activity toward ORR, the polarization curves of the catalysts were measured in O$_2$-saturated 0.1 M HClO$_4$ solution at a scan rate of 5 mV s^{-1} and a rotation rate of 1600 rpm (Fig. 5c). The Pt/TiO$_2$ displays extremely low ORR catalytic activity in acidic medium, presumably due to the low electronic conductivity of pristine TiO$_2$ support. EIS measurement represents the electron-transfer
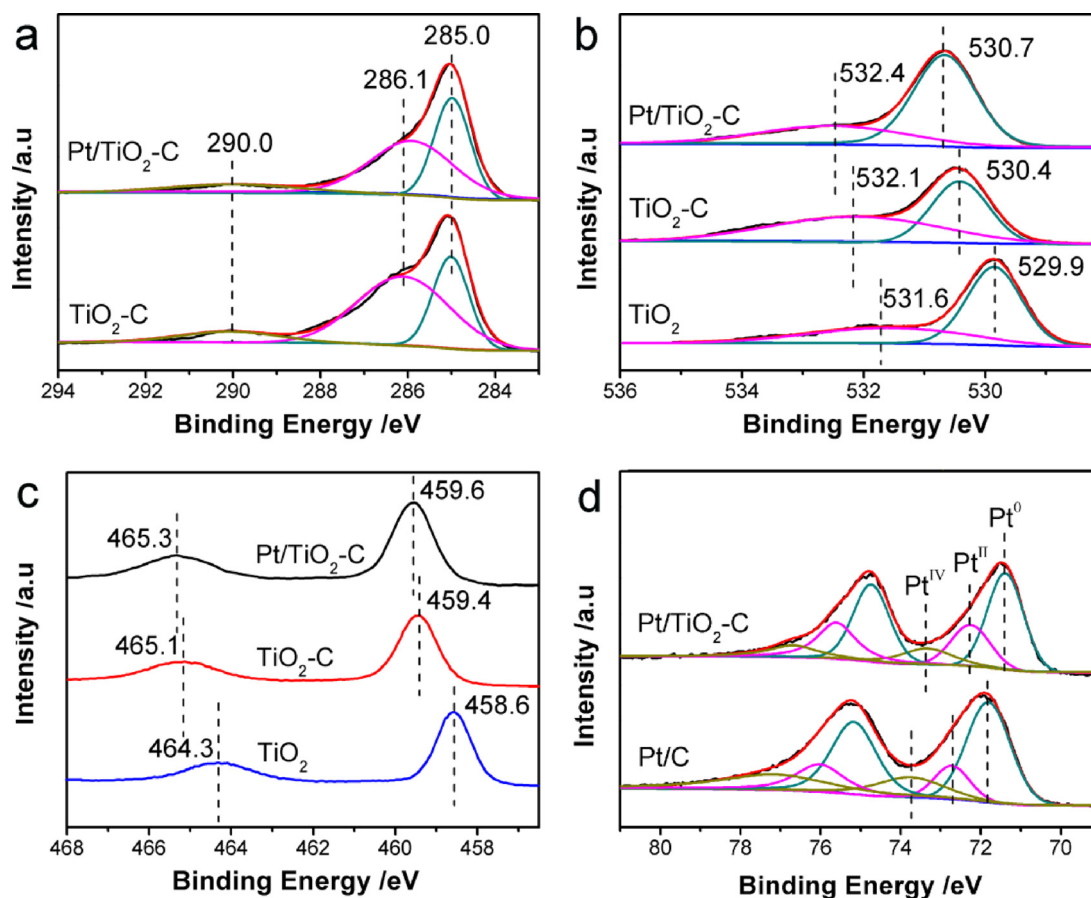
Fig. 3. High-resolution XPS results of (a) C 1 s, (b) O 1 s, (c) Ti 2p, and (d) Pt 4f in the Pt/TiO₂-C catalyst.

resistance across the electrode/electrolyte (Fig. S5). The Nyquist plot verifies the low conductivity of TiO_2 and Pt/TiO_2 as compared to TiO_2-C and Pt/TiO_2-C, indicating that the conductivity of TiO_2 semiconductor can be effectively improved by carbon incorporation. The Pt/TiO₂-C presents more positive onset potential ($E_O = 0.972$ V) and half-wave potential ($E_{1/2} = 0.876$ V) than Com. Pt/C ($E_O = 0.928$ and $E_{1/2} = 0.827$ V), versus reversible hydrogen electrode (RHE). Similar trend is observed when comparing the electrocatalytic activity of these samples toward ORR in alkaline medium (Fig. S6). It should be noted that, even for the same Com. Pt/C catalysts, the potential value of E_O or $E_{1/2}$ varied under different testing conditions, such as loading mass of Pt, electrolyte type, flow rate of gas, scan rate, or some cases using

Ohmic drop correction, etc. Hence the main experiment conditions and the results of Com. Pt in each report are also provided in Table S2 to compare the change in electrocatalytic activity after TiO_2 incorporation. The ~49 mV positive shift of $E_{1/2}$ is found to be much higher than the previous reported values for loading comparable mass of Pt on TiO_2-containing carbon.

The controlled experiment was conducted to demonstrate the advantage of photochemical strategy by comparing with the typical reduction methods using polyol and H_2 as reduction reagents. The Pt/TiO₂-C (polyol) and Pt/TiO₂-C (H_2) electrocatalysts exhibit comparable ORR activity to Com. Pt/C, however they are definitely less efficient than the Pt/TiO₂-C from photochemical system (Fig. S7). As above-
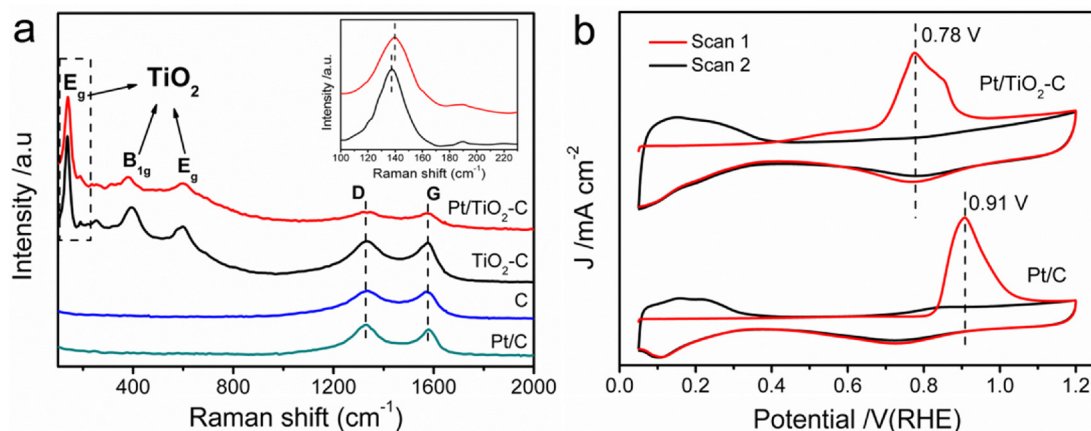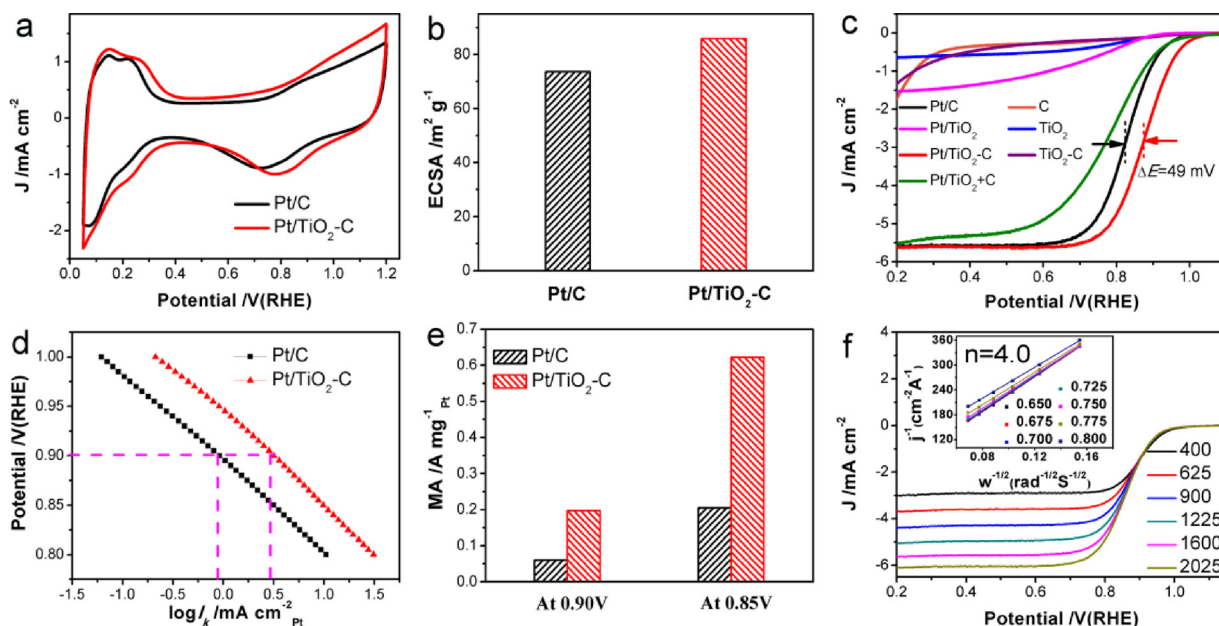

Fig. 4. (a) Raman spectra of Pt/C, carbon black, TiO₂-C, and Pt/TiO₂-C composite. (b) CO-stripping characteristic in acid conditions (0.1 M HClO₄) for Pt/TiO₂-C and commercial Pt/C.

Fig. 5. (a) Cyclic voltammetry curves of commercial Pt/C and Pt/TiO$_2$-C in N$_2$-saturated 0.1 M HClO$_4$ at room temperature at a scan rate of 50 mV s^{-1}. (b) Comparison of ECSA values. (c) ORR polarization curves of catalysts in O$_2$-saturated 0.1 M HClO$_4$ at a scan rate of 5 mV s^{-1} and a rotation rate of 1600 rpm. The Pt/TiO$_2$ + C catalyst is prepared for comparison by depositing Pt on the physical mixture of carbon black and TiO$_2$. (d) Tafel plots derived from the polarization curves for Pt/C and Pt/TiO$_2$-C. (e) Comparison of mass activity (MA) at 0.85 and 0.9 V. (f) The ORR polarization curves of Pt/TiO$_2$-C in O$_2$-saturated 0.1 M HClO$_4$ at various rotation rates. The inset is the Koutecky–Levich plots from polarization curves at different potentials.

mentioned, the Pt NPs are inclined to growing around the TiO$_2$ NPs to induce the SMSI effect owing to direct reduction by the photogenerated electrons on the TiO$_2$ surface. Differently, the Pt NPs produced by typical reduction methods are randomly dispersed on the TiO$_2$-C support. Through this comparison, it can be deduced that the photochemical strategy favors the ORR activity of Pt electrocatalyst from the aspect of generating direct electronic interactions with TiO$_2$-C support.

In order to explain the superiority of well-dispersed TiO$_2$-C composite support, the mixture support of carbon black and TiO$_2$ is prepared by mechanically blending and labeled as "TiO$_2$ + C" for comparison. The blended "TiO$_2$ + C" support contains the same proportion of TiO$_2$ to C, so it yields a similar amount of Pt as compared to the TiO$_2$-C composite. However, the remarkably enhanced ORR activity of Pt electrocatalysts is only achieved when using TiO$_2$-C composite support with uniform dispersion of TiO$_2$ NCs on the carbon surface. The difference can be attributed to the formation of more interfacial interaction between TiO$_2$ and C in the composite support, which makes the electrocatalytic ORR reaction more efficient than that in physical mixture. The comparison in Nyquist plot further reflects the less improvement in the TiO$_2$ conductivity by mechanically blending with carbon material than that by liquid-phase assembly (Fig. S5). To study the contribution of TiO$_2$-C support to the electrocatalytic efficiency of Pt catalysts, the weight ratio of Pt NPs was reduced by half, i.e., from 6.9% to 3.5% by ICP-MS measurement. The crystal size of Pt NPs is estimated to be ~3.9 nm using Pt(111) diffraction peak (Fig. S8), similar to that of 6.9% Pt/TiO$_2$-C. When normalizing the mass of the loaded Pt, the mass of TiO$_2$-C on the working electrode would be ~2 times of the original value. The ORR polarization curves were thoroughly overlapped with similar values of E_O and $E_{1/2}$ (Fig. S9). This indicates the inertness of TiO$_2$-C support toward electrocatalytic ORR. Thus it can be deduced that the improvement of electrocatalytic activity does not originate from the contribution by TiO$_2$ itself but the electronic interactions with Pt catalysts.

The Tafel slopes for the kinetic current in Fig. 5d were calculated from the corresponding polarization curves by the Koutecky–Levich (K–L) equation. The Tafel slope of Pt/TiO$_2$-C (68 mV dec^{-1}) is close to that of Com. Pt/C (71 mV dec^{-1}), which indicates the comparable

kinetic behavior and kinetic current density. Then the mass activity (MA) is derived and plotted in Fig. 5e. The Pt/TiO$_2$-C exhibits a MA of 0.205 A mg^{-1}, which is ~3.4 times greater than that of Com. Pt/C catalyst (0.06 A mg^{-1}) at 0.9 V (vs RHE). In addition, Fig. 5f shows the ORR polarization curves of Pt/TiO$_2$-C in O$_2$-saturated 0.1 M HClO$_4$ at various rotation rates. The diffusion-limiting current density increased proportionally with the rotating rate due to the shortened diffusion distance at higher rate. The K–L plots at various potentials display an overlapped shape with good linearity over the examined potential range. The number of transferred electrons was calculated to be 4.0 from the slopes. The same result is obtained from the measurement in O$_2$-saturated 0.1 M KOH (Fig. S10). This implied the typical first-order reaction kinetics with a direct 4-electron transfer mechanism under both acidic and alkaline conditions.

The electrochemical stability of Pt/TiO$_2$-C was evaluated by accelerated durability test (ADT), which was performed in N$_2$-saturated 0.1 M HClO$_4$ solutions at a scan rate of 100 mV s^{-1}. The CV and LSV curves before and after room-temperature ADT (RT-ADT) were compared in Fig. 6. The $E_{1/2}$ value of Pt/TiO$_2$-C catalyst shows negative shift of only 1 mV, whereas that of Com. Pt/C decreased by 24 mV after 10,000 cycles. The calculated ECSA and MA of Com. Pt/C seriously decreased to 10.2 and 33.3% of the original values, respectively. In contrast, the Pt/TiO$_2$-C catalysts possessed a good retention of electrocatalytic activity, a much slighter loss as 0.8% of ECSA and 0.9% of MA. Furthermore, the decreased percentages of the Pt/TiO$_2$-C catalysts experienced during high-temperature ADT (HT-ADT) at 60 °C are 17.1% for ECSA and 28.8% for MA, appearing to be more stable than Com. Pt/C (40.2 and 58.3% loss of ECSA and MA). The morphology of Pt/TiO$_2$-C catalysts after ADT was observed by TEM and HRTEM. After 10,000 cycles, the Pt NPs, with only a slight change in particle size from 3.2 to 4.1 nm, well maintained the uniform dispersion around the TiO$_2$ surface (Fig. 7).

The above results indicate that the Pt catalysts on TiO$_2$-C support possess more superior ORR electrocatalytic performance than Com. Pt/C in terms of activity and stability. As reported by literatures, the carbon corrosion and weak metal-support interactions play a dominant role in threatening the long-term operation of Pt-based catalysts under
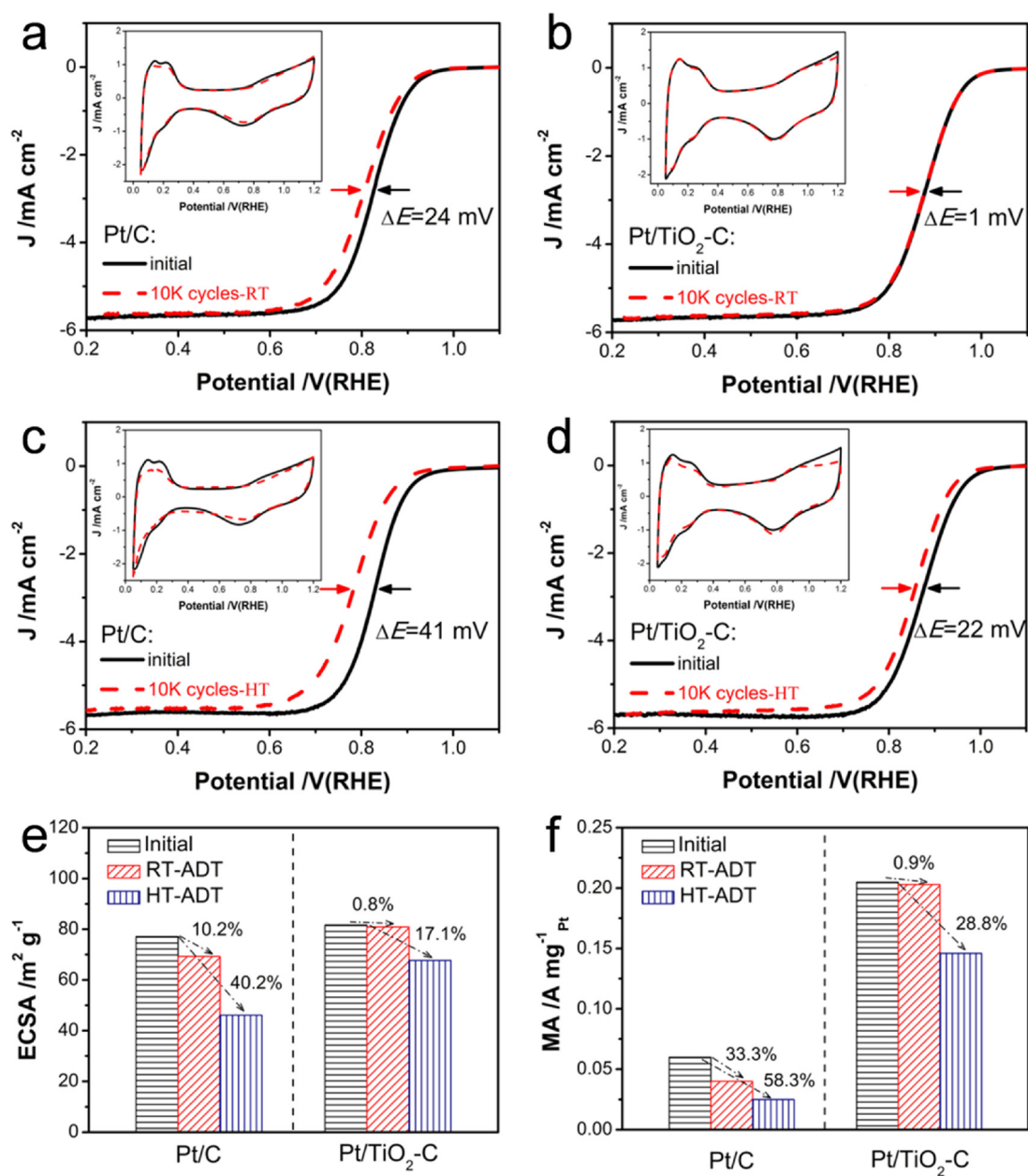
Fig. 6. CV and LSV curves of commercial Pt/C (a) and Pt/TiO$_2$-C (b) before and after RT-ADT in N$_2$-saturated 0.1 M HClO$_4$ solutions at a scan rate of 100 mV s^{-1}. CV and LSV curves of Pt/C (c) and commercial Pt/TiO$_2$-C (d) before and after HT-ADT at 60 °C. The changes on ECSA (e) and MA (f) before and after RT-ADT and HT-ADT.
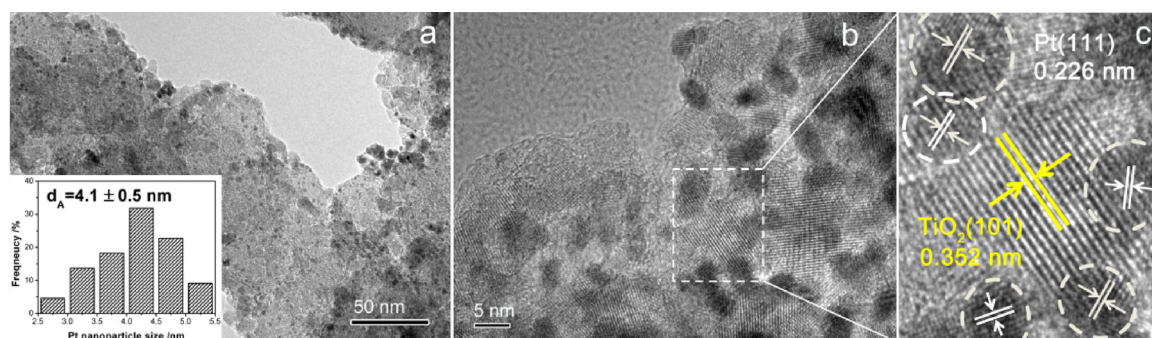
Fig. 7. TEM (a) and HRTEM (b) images of Pt/TiO$_2$-C after durability test of 10,000 cycles. (c) The magnification of the selected area in (b). The inset in (a) is the Pt particle size distribution.

electrochemical conditions, especially in acidic medium and high-temperature environment [35–37]. In this regard, the achievement in Pt/TiO₂-C system might be attributed to the TiO₂-induced SMSI effect strongly anchoring Pt NPs to facilitate the electron transfer as well as prevent the migration and aggregation.

4. Conclusions

In this work, we designed a TiO₂-C composite support with well-dispersed TiO₂ NCs on carbon surface. Then the ultrafine Pt NPs were in situ reduced by the photogenerated electrons on TiO₂ surface so that most of them surrounded the TiO₂ NCs with well-dispersion. It was convincing that the decoration of well-dispersed TiO₂ NCs significantly improved the corrosion resistance of carbon materials against strong acidic medium and high-temperature environment. Moreover, in the presence of TiO₂ NCs, the interactions with carbon networks and Pt NPs would strengthen the SMSI effect, which facilitated the electron transfer during catalytic reactions as well as strongly anchored Pt NPs to prevent the migration and aggregation during cycling test. As a result, we just used the cheap carbon black and pristine TiO₂, but the as-prepared Pt NPs electrocatalysts achieved higher ORR catalytic performance than Com. Pt/C through the comprehensive comparisons in E_O, $E_{1/2}$, ECSA, and durability at both room and high temperature. It was expected that the designed TiO₂-decorated carbon in this work would emerge to be a superior support material as well as photoelectron contributor for anchoring metal catalysts to dramatically enhance their activity and durability toward diverse catalytic reactions.

Acknowledgements

Appendix A. Supplementary data

Supplementary material related to this article can be found, in the online version, at doi:https://doi.org/10.1016/j.apcatb.2018.05.085.

References

[1] M. Shao, Q. Chang, J.P. Dodelet, R. Chenitz, Recent advances in electrocatalysts for oxygen reduction reaction, Chem. Rev. 116 (2016) 3594–3657.

[2] G.-R. Zhang, S. Wöllner, Hollowed structured PtNi bifunctional electrocatalyst with record low total overpotential for oxygen reduction and oxygen evolution reactions, Appl. Catal. B Environ. 222 (2018) 26–34.

[3] S. Zhang, Y. Hao, D. Su, V.V. Doan-Nguyen, Y. Wu, J. Li, S. Sun, C.B. Murray, Monodisperse core/shell Ni/FePt nanoparticles and their conversion to Ni/Pt to catalyze oxygen reduction, J. Am. Chem. Soc. 136 (2014) 15921–15924.

[4] Q. Li, X. Wen, G. Wu, H.T. Chung, R. Gao, P. Zelenay, High-activity PtRuPd/C catalyst for direct dimethyl ether fuel cells, Angew. Chem. Int. Ed. Engl. 54 (2015) 7524–7528.

[5] D. Wang, Y. Yu, J. Zhu, S. Liu, D.A. Muller, H.D. Abruna, Morphology and activity tuning of Cu₃Pt/C ordered intermetallic nanoparticles by selective electrochemical dealloying, Nano Lett. 15 (2015) 1343–1348.

[6] M.-C. Tsai, T.-T. Nguyen, N.G. Akalework, C.-J. Pan, J. Rick, Y.-F. Liao, W.-N. Su, B.-J. Hwang, Interplay between molybdenum dopant and oxygen vacancies in a TiO₂ support enhances the oxygen reduction reaction, ACS Catal. 6 (2016) 6551–6559.

[7] K.M. Yeo, S. Choi, R.M. Anisur, J. Kim, I.S. Lee, Surfactant-free platinum-on-gold nanodendrites with enhanced catalytic performance for oxygen reduction, Angew. Chem. Int. Ed. Engl. 50 (2011) 745–748.

[8] L. Li, L. Hu, J. Li, Z. Wei, Enhanced stability of Pt nanoparticle electrocatalysts for fuel cells, Nano Res. 8 (2015) 418–440.

[9] J.S. Bunch, A.M. van der Zande, S.S. Verbridge, I.W. Frank, D.M. Tanenbaum, J.M. Parpia, H.G. Craighead, P.L. McEuen, Electromechanical resonators from graphene sheets, Science 315 (2007) 490–493.

[10] V. Beermann, M. Gocyla, E. Willinger, S. Rudi, M. Heggen, R.E. Dunin-Borkowski, M.G. Willinger, P. Strasser, Rh-Doped Pt–Ni octahedral nanoparticles:

[11] understanding the correlation between elemental distribution, oxygen reduction reaction, and shape stability, Nano Lett. 16 (2016) 1719–1725.

[11] B. Wu, D. Liu, S. Mubeen, T.T. Chuong, M. Moskovits, G.D. Stucky, Anisotropic growth of TiO₂ onto gold nanorods for plasmon-enhanced hydrogen production from water reduction, J. Am. Chem. Soc. 138 (2016) 1114–1117.

[12] X. Liu, G. Dong, S. Li, G. Lu, Y. Bi, Direct observation of charge separation on anatase TiO₂ crystals with selectively etched {001} facets, J. Am. Chem. Soc. 138 (2016) 2917–2920.

[13] S. Wang, B.Y. Guan, L. Yu, X.W.D. Lou, Rational design of three-layered TiO₂@ carbon@ MoS₂ hierarchical nanotubes for enhanced lithium storage, Adv. Mater. 29 (2017) 1702724.

[14] L. Pan, S. Wang, J. Xie, L. Wang, X. Zhang, J.-J. Zou, Constructing TiO₂ pn homojunction for photoelectrochemical and photocatalytic hydrogen generatio, Nano Energy 28 (2016) 296–303.

[15] M. Tahir, L. Pan, F. Idrees, X. Zhang, L. Wang, J.-J. Zou, Z.L. Wang, Electrocatalytic oxygen evolution reaction for energy conversion and storage: a comprehensive review, Nano Energy 37 (2017) 136–157.

[16] Y. Ji, Yi. Cho, Y. Jeon, C. Lee, D.-H. Park, Y.-G. Shul, Design of active Pt on TiO₂ based nanofibrous cathode for superior PEMFC performance and durability at high temperature, Appl. Catal. B Environ. 204 (2017) 421–429.

[17] C.W. Liu, H.S. Chen, C.M. Lai, J.N. Lin, L.D. Tsai, K.W. Wang, Promotion of oxygen reduction reaction durability of carbon-supported PtAu catalysts by surface segregation and TiO₂ addition, ACS Appl. Mater. Interfaces 6 (2014) 1589–1594.

[18] M. Cao, Z. Tang, Q. Liu, Y. Xu, M. Chen, H. Lin, Y. Li, E. Gross, Q. Zhang, The synergy between metal facet and oxide support facet for enhanced catalytic performance: the case of Pd–TiO₂, Nano Lett. 16 (2016) 5298–5302.

[19] R. Long, K. Mao, M. Gong, S. Zhou, J. Hu, M. Zhi, Y. You, S. Bai, J. Jiang, Q. Zhang, X. Wu, Y. Xiong, Tunable oxygen activation for catalytic organic oxidation: schottky junction versus plasmonic effects, Angew. Chem. Int. Ed. Engl. 53 (2014) 3205–3209.

[20] D. Widmann, R.J. Behm, Activation of molecular oxygen and the nature of the active oxygen species for CO oxidation on oxide supported Au catalysts, Acc. Chem. Res. 47 (2014) 740–749.

[21] V.T. Ho, C.J. Pan, J. Rick, W.N. Su, B.J. Hwang, Nanostructured $Ti_{0.7}Mo_{0.3}O_2$ support enhances electron transfer to Pt: high-performance catalyst for oxygen reduction reaction, J. Am. Chem. Soc. 133 (2011) 11716–11724.

[22] N.G. Akalework, C.-J. Pan, W.-N. Su, J. Rick, M.-C. Tsai, J.-F. Lee, J.-M. Lin, L.-D. Tsai, B.-J. Hwang, Ultrathin TiO₂-coated MWCNTs with excellent conductivity and SMSI nature as Pt catalyst support for oxygen reduction reaction in PEMFCs, J. Mater. Chem. 22 (2012) 20977.

[23] G. Chen, K.A. Kuttiyiel, D. Su, M. Li, C.-H. Wang, D. Buceta, C. Du, Y. Gao, G. Yin, K. Sasaki, M.B. Vukmirovic, R.R. Adzic, Oxygen reduction kinetics on Pt monolayer shell highly affected by the structure of bimetallic AuNi cores, Chem. Mater. 28 (2016) 5274–5281.

[24] D.S. Choi, A.W. Robertson, J.H. Warner, S.O. Kim, H. Kim, Low-temperature chemical vapor deposition synthesis of Pt–Co alloyed nanoparticles with enhanced oxygen reduction reaction catalysis, Adv. Mater. 28 (2016) 7115–7122.

[25] X. Wang, L. Figueroa-Cosme, X. Yang, M. Luo, J. Liu, Z. Xie, Y. Xia, Pt-Based icosahedral nanocages: using a combination of {111} facets, twin defects, and ultra-thin walls to greatly enhance their activity toward oxygen reduction, Nano Lett. 16 (2016) 1467–1471.

[26] A. Zhao, J. Masa, W. Xia, Oxygen-deficient titania as alternative support for Pt catalysts for the oxygen reduction reaction, J. Energy Chem. 23 (2014) 701–707.

[27] M. Wang, Z. Wang, L. Wei, J. Li, X. Zhao, Catalytic performance and synthesis of a Pt/graphene-TiO₂ catalyst using an environmentally friendly microwave-assisted solvothermal method, Chin. J. Catal. 38 (2017) 1680–1687.

[28] B.-J. Hsieh, M.-C. Tsai, C.-J. Pan, W.-N. Su, J. Rick, H.-L. Chou, J.-F. Lee, B.-J. Hwang, Tuning metal support interactions enhances the activity and durability of TiO₂-supported Pt nanocatalysts, Electrochim. Acta 224 (2017) 452–459.

[29] X. Tian, J. Luo, H. Nan, H. Zou, R. Chen, T. Shu, X. Li, Y. Li, H. Song, S. Liao, R.R. Adzic, Transition metal nitride coated with atomic layers of Pt as a low-cost, highly stable electrocatalyst for the oxygen reduction reaction, J. Am. Chem. Soc. 138 (2016) 1575–1583.

[30] G. Niu, M. Zhou, X. Yang, J. Park, N. Lu, J. Wang, M.J. Kim, L. Wang, Y. Xia, Synthesis of Pt–Ni octahedra in continuous-flow droplet reactors for the scalable production of highly active catalysts toward oxygen reduction, Nano Lett. 16 (2016) 3850–3857.

[31] N.T. Nguyen, M. Altomare, J.E. Yoo, N. Taccardi, P. Schmuki, Noble metals on anodic TiO₂ nanotube mouths: thermal dewetting of minimal PtCo-catalyst loading leads to significantly enhanced photocatalytic H₂ generation, Adv. Energy Mater. 6 (2016) 1501926.

[32] Y. Sui, S. Liu, T. Li, Q. Liu, T. Jiang, Y. Guo, J.-L. Luo, Atomically dispersed Pt on specific TiO₂ facets for photocatalytic H₂ evolution, J. Catal. 353 (2017) 250–255.

[33] C. Meng, B. Wang, Z. Gao, Z. Liu, Q. Zhang, J. Zhai, Insight into the role of surface wettability in electrocatalytic hydrogen evolution reactions using light-sensitive nanotubular TiO₂ supported Pt electrodes, Sci. Rep. 7 (2017) 41825.

[34] B. Liu, H.M. Chen, C. Liu, S.C. Andrews, C. Hahn, P. Yang, Large-scale synthesis of transition-metal-doped TiO₂ nanowires with controllable overpotential, J. Am. Chem. Soc. 135 (2013) 9995–9998.

[35] D.N. Pei, L. Gong, A.Y. Zhang, X. Zhang, J.J. Chen, Y. Mu, H.Q. Yu, Defective titanium dioxide single crystals exposed by high-energy {001} facets for efficient oxygen reduction, Nat. Commun. 6 (2015) 8696.

[36] J.-H. Kim, G. Kwon, H. Lim, C. Zhu, H. You, Y.-T. Kim, Effects of transition metal doping in Pt/M-TiO₂ (M = V, Cr, and Nb) on oxygen reduction reaction activity, J. Power Sources 320 (2016) 188–195.

[37] M. Kim, C. Kwon, K. Eom, J. Kim, E. Cho, Electrospun Nb-doped TiO₂ nanofiber

support for Pt nanoparticles with high electrocatalytic activity and durability, Sci. Rep. 7 (2017) 44411.

[38] F. Ando, T. Tanabe, T. Gunji, T. Tsuda, S. Kaneko, T. Takeda, T. Ohsaka, F. Matsumoto, Improvement of ORR activity and durability of Pt electrocatalyst nanoparticles anchored on TiO_2/Cup-stacked carbon nanotube in acidic aqueous media, Electrochim. Acta 232 (2017) 404–413.

[39] Y. Chang, C. Yuan, Y. Li, C. Liu, T. Wu, B. Zeng, Y. Xu, L. Dai, Controllable fabrication of a N and B co-doped carbon shell on the surface of TiO_2 as a support for boosting the electrochemical performances, J. Mater. Chem. A 5 (2017) 1672–1678.

[40] R. Badam, R. Vedarajan, K. Okaya, K. Matsutani, N. Matsumi, Sacrificial reducing agent Free photo-generation of platinum nano particle over Carbon/TiO_2 for highly efficient oxygen reduction reaction, Sci. Rep. 6 (2016) 37006.

[41] J. He, Y. He, Y. Fan, B. Zhang, Y. Du, J. Wang, P. Xu, Conjugated polymer-mediated synthesis of nitrogen-doped carbon nanoribbons for oxygen reduction reaction, Carbon 124 (2017) 630–636.

[42] K. Song, Z. Zou, D. Wang, B. Tan, J. Wang, J. Chen, T. Li, Microporous organic polymers derived microporous carbon supported Pd catalysts for oxygen reduction reaction: impact of framework and heteroatom, J. Phys. Chem. C 120 (2016) 2187–2197.

[43] X. Wan, C. Zhou, J. Chen, W. Deng, Q. Zhang, Y. Yang, Y. Wang, Base-free aerobic oxidation of 5-hydroxymethyl-furfural to 2, 5-furandicarboxylic acid in water catalyzed by functionalized carbon nanotube-supported Au–Pd alloy nanoparticles, ACS Catal. 4 (2014) 2175–2185.

[44] M.C. Tsai, T.T. Nguyen, N.G. Akalework, C.J. Pan, J. Rick, Y.F. Liao, W.N. Su, B.J. Hwang, Interplay between molybdenum dopant and oxygen vacancies in a TiO_2 support enhances the oxygen reduction reaction, ACS Catal. 6 (2016) 6551–6559.

[45] K. Kinoshita, Particle size effects for oxygen reduction on highly dispersed platinum in acid electrolytes, J. Electrochem. Soc. 137 (1990) 845–848.

[46] F.J. Perez-Alonso, D.N. McCarthy, A. Nierhoff, P. Hernandez-Fernandez, C. Strebel, I.E. Stephens, J.H. Nielsen, I. Chorkendorff, The effect of size on the oxygen electroreduction activity of mass-selected platinum nanoparticles, Angew. Chem. Int. Ed. Engl. 51 (2012) 4641–4643.

[47] S.H. Joo, K. Kwon, D.J. You, C. Pak, H. Chang, J.M. Kim, Preparation of high loading Pt nanoparticles on ordered mesoporous carbon with a controlled Pt size and its effects on oxygen reduction and methanol oxidation reactions, Electrochim. Acta 54 (2009) 5746–5753.

[48] K. Pandiselvi, H. Fang, X. Huang, J. Wang, X. Xu, T. Li, Constructing a novel carbon nitride/polyaniline/ZnO ternary heterostructure with enhanced photocatalytic performance using exfoliated carbon nitride nanosheets as supports, J. Hazard. Mater. 314 (2016) 67–77.

[49] Z. Xu, C. Zhuang, Z. Zou, J. Wang, X. Xu, T. Peng, Enhanced photocatalytic activity by the construction of a TiO_2/carbon nitride nanosheets heterostructure with high surface area via direct interfacial assembly, Nano Res. 10 (2017) 2193–2209.

[50] H. Cheng, X. Feng, D. Wang, M. Xu, K. Pandiselvi, J. Wang, Z. Zou, T. Li, Synthesis of highly stable and methanol-tolerant electrocatalyst for oxygen reduction: Co supporting on N-doped-C hybridized TiO_2, Electrochim. Acta 180 (2015) 564–573.

[51] J. Ma, A. Habrioux, N. Alonso-Vante, The effect of substrates at cathodes in low-temperature fuel cells, ChemElectroChem 1 (2014) 37–46.

[52] S. Liu, W. Xiao, J. Wang, J. Zhu, Z. Wu, H. Xin, D. Wang, Ultralow content of Pt on Pd–Co–Cu/C ternary nanoparticles with excellent electrocatalytic activity and durability for the oxygen reduction reaction, Nano Energy 27 (2016) 475–481.

[53] D. Wang, H.L. Xin, Y. Yu, H. Wang, E. Rus, D.A. Muller, H.D. Abruna, Pt-Decorated PdCo@Pd/C core−shell nanoparticles with enhanced stability and electrocatalytic activity for the oxygen reduction reaction, J. Am. Chem. Soc. 132 (2010) 17664–17666.

[54] M. Li, Z. Zhao, T. Cheng, A. Fortunelli, C.Y. Chen, R. Yu, Q. Zhang, L. Gu, B.V. Merinov, Z. Lin, E. Zhu, T. Yu, Q. Jia, J. Guo, L. Zhang, W.A. Goddard 3rd, Y. Huang, X. Duan, Ultrafine jagged platinum nanowires enable ultrahigh mass activity for the oxygen reduction reaction, Science 354 (2016) 1414–1419.

[55] L. Bu, N. Zhang, S. Guo, X. Zhang, J. Li, J. Yao, T. Wu, G. Lu, J.Y. Ma, D. Su, X. Huang, Biaxially strained PtPb/Pt core/shell nanoplate boosts oxygen reduction catalysis, Science 354 (2016) 1410–1414.

[56] D.S. He, D. He, J. Wang, Y. Lin, P. Yin, X. Hong, Y. Wu, Y. Li, Ultrathin icosahedral Pt-enriched nanocage with excellent oxygen reduction reaction activity, J. Am. Chem. Soc. 138 (2016) 1494–1497.